Radiative Transfer in Water Clouds in the Infrared Region[1]

GIICHI YAMAMOTO, MASAYUKI TANAKA AND SHOJI ASANO

Geophysical Institute, Tohoku University, Sendai, Japan

(Manuscript received 15 September 1969, in revised form 8 December 1969)

ABSTRACT

The problem of diffuse reflection, transmission and emission of infrared radiation by water clouds is investigated in the wavelength region from 5–50 μ. The drop-size distribution of clouds is assumed to be that of altostratus measured by Diem. The phase function and other optical properties of the clouds are estimated from the value of the refractive index of water proposed by Pontier and Dechambenoy. Radiative processes due to both cloud droplets and water vapor in the cloud are taken into account, and a method of averaging the solution over a spectral interval including a number of absorption lines is developed.

1. Introduction

Radiative transfer in water clouds in the 10 μ window region was studied by Yamamoto *et al.* (1966) by a method based on Chandrasekhar's (1950) principle of invariance. As a continuation of that work, we have studied in this paper radiative transfer of water clouds in the whole infrared region by the same method as the one used in the previous work. The difference is that in the window region it is only necessary to take into account scattering and absorption by cloud droplets, whereas in the band regions of the infrared it is necessary to take into account not only scattering and absorption by cloud droplets but also absorption by gaseous constituents in clouds. Consequently, because of the line structure of the absorption bands of gases, a useful solution of the equation of radiative transfer should be one which is averaged over the wavelength. This paper shows a method of averaging the solution over a spectral interval and the resulting solution for the main infrared region from 5–50 μ.

2. Optical properties of clouds

In order to carry out this research it is necessary to evaluate the phase function at each wavelength, i.e., evaluate the local scattering properties of clouds. Assuming that water clouds are composed of spherical water droplets, we can evaluate the phase function as functions of the size distribution of the cloud droplets and the complex refractive index of water.

There are several investigations on the complex refractive index of water in the infrared region. Fig. 1 shows values of the real part of the complex refractive index of water in the infrared region evaluated by Kislovskii (1959), Pontier and Dechambenoy (1966), and Irvine and Pollack (1968). In the far infrared region beyond 15 μ, the values of Pontier and Dechambenoy are smaller than those by Kislovskii or Irvine and Pollack. Here it should by noticed that the values given by Pontier and Dechambenoy are based on their latest measurements, while those given by other workers are derived from data on reflective power compiled by Dorsey in 1940.

Fig. 2 shows the corresponding values of the imaginary part of the refractive index. They are not coincident in the region beyond 15 μ. The values given by Kislovskii are based on absorption measurements by Plyler and Acquista (1954), while those by Irvine and Pollack are due to the data compiled by Centeno (1941) for the 15 μ band of water and to those measured by Draegert *et al.* (1966) for longer wavelengths. Values given by Pontier and Dechambenoy are the only ones based on their own measurements. In the following study we shall use values provided by Pontier and Dechambenoy for both real and imaginary parts of the refractive index, because they are based on the latest measurements.

The phase function of clouds is then obtained straightforwardly and is not shown here.[2]

3. Process of averaging the solution over a spectral interval

In this study we shall take into account the absorption by water vapor in the cloud. Then the albedo ω_ν for single scattering of the cloud at wavenumber ν becomes

$$\omega_\nu = \sigma_{s,\nu}/\sigma_\nu, \tag{1}$$

and

$$\sigma_\nu = \sigma_{s,\nu} + \sigma_{a,\nu} + k_\nu, \tag{2}$$

[1] This work was supported by the Environmental Science Services Administration under Contract E-24-69(N).

[2] The values of the phase function used in this investigation are available on request.

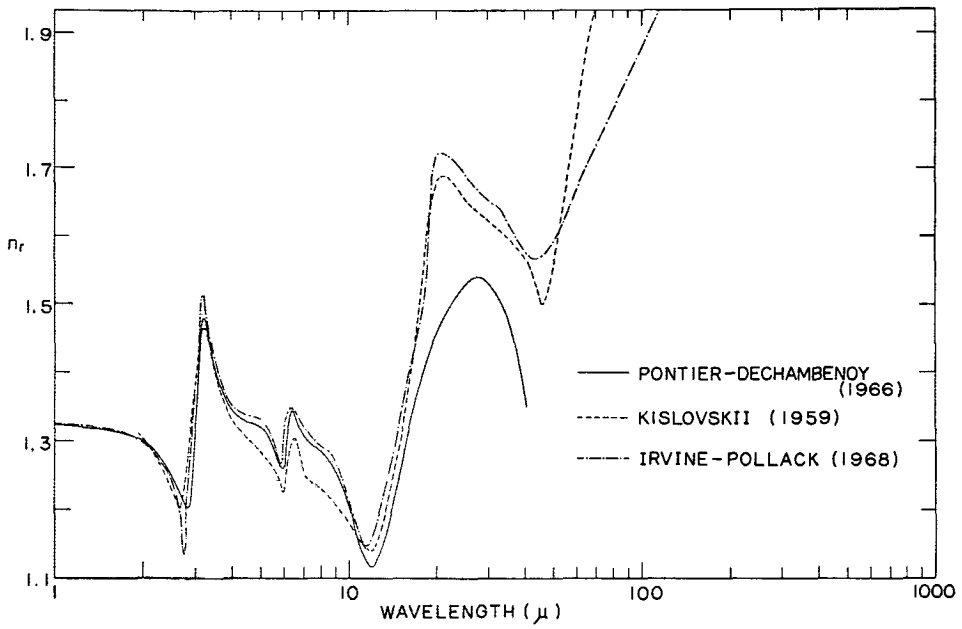

FIG. 1. Real part of the refractive index of water vs wavelength.

where $\sigma_{s,\nu}$ and $\sigma_{a,\nu}$ are the volume scattering and absorption coefficients, respectively, due to cloud droplets, k_ν the volume absorption coefficient of water vapor, and σ_ν the resultant extinction coefficient of the cloud. We shall consider a plane-parallel cloud layer with a dry atmosphere outside. The monochromatic optical thickness and the geometrical distance from the top of the cloud to some level in it are denoted by τ and x, respectively. The total optical and geometrical thicknesses of the cloud are given by τ_1 and x_1, respectively. The configuration of the model is shown in Fig. 3. As in the previous work (Yamamoto *et al.*, 1966), the quantities in which we are mostly interested are $I_\nu^s(\tau_1; -\mu)$, the reflected intensity at the cloud bottom; $I_\nu^s(0; +\mu)$, the transmitted intensity at the cloud top; and $I_\nu^e(0; +\mu)$ $[=I_\nu^e(\tau_1; -\mu)]$, the emitted intensity (Fig. 3). These quantities can be expressed in terms of the scattering function S_ν, the transmission function T_ν and the emission function E_ν, which in turn satisfy the simultaneous integral equations [Eqs. (12), (13) and (21) of the paper

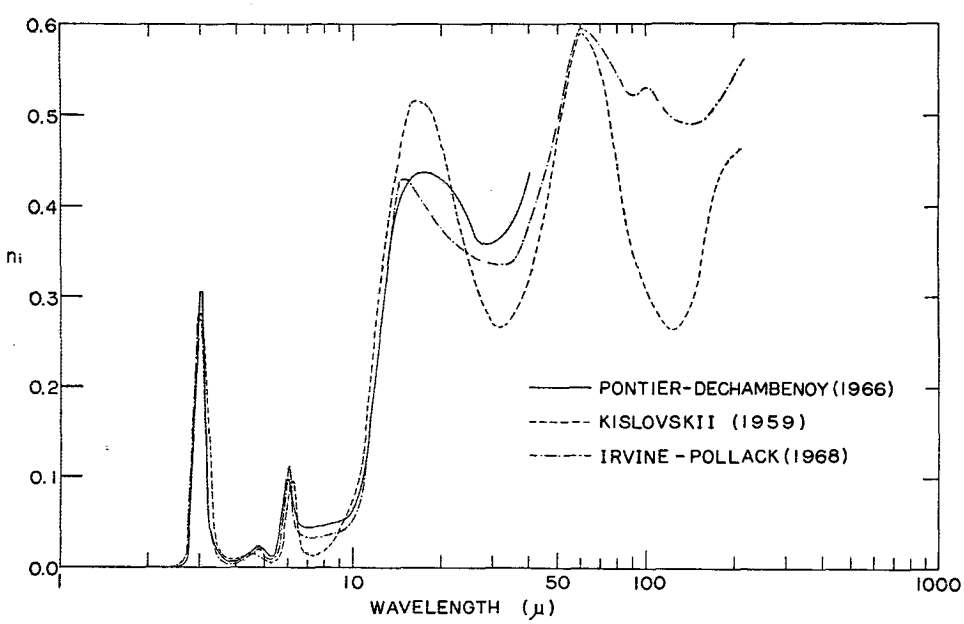

FIG. 2. Imaginary part of the refractive index of water vs wavelength.

by Yamamoto *et al.*]. As in the previous paper, we shall expand S_ν, T_ν and E_ν in power series of ω_ν in the form

$$S_\nu(x_1;\mu,\mu')=\sum_{n=1}^{\infty}\omega_\nu{}^n S_\nu{}^{(n)}(x_1;\mu,\mu')=\sum_{n=1}^{\infty}\mathcal{S}_\nu{}^{(n)}(x_1;\mu,\mu'), \tag{3}$$

$$T_\nu(x_1;\mu,\mu')=\sum_{n=1}^{\infty}\omega_\nu{}^n T_\nu{}^{(n)}(x_1;\mu,\mu')=\sum_{n=1}^{\infty}\mathcal{J}_\nu{}^{(n)}(x_1;\mu,\mu'), \tag{4}$$

$$E_\nu(x_1;\mu)=\sum_{n=0}^{\infty}\omega_\nu{}^n E_\nu{}^{(n)}(x_1;\mu)=\sum_{n=0}^{\infty}\mathcal{E}_\nu{}^{(n)}(x_1;\mu). \tag{5}$$

Here the total geometrical thickness $x_1(=\tau_1/\sigma_\nu)$ is used in place of the total optical thickness τ_1. Substituting (3) into (13) of the previous paper, for instance, we have the recursion relations for $\mathcal{S}_\nu{}^{(n)}$ i.e.,

$$(1/\mu+1/\mu')\mathcal{S}_\nu{}^{(1)}(x_1;\mu,\mu')=\omega_\nu\{1-\exp[-\sigma_\nu x_1(1/\mu+1/\mu')]\}p^{(0)}(\mu,-\mu'),$$

$$\begin{aligned}(1/\mu+1/\mu')&\mathcal{S}_\nu{}^{(2)}(x_1;\mu,\mu')\\ =&\frac{\omega_\nu}{2}\int_0^1 p^{(0)}(\mu,\mu'')\mathcal{S}_\nu{}^{(1)}(x_1;\mu'',\mu')\frac{d\mu''}{\mu''}+\frac{\omega_\nu}{2}\int_0^1\mathcal{S}_\nu{}^{(1)}(x_1;\mu,\mu'')p^{(0)}(-\mu'',-\mu')\frac{d\mu''}{\mu''}\\ &-\frac{\omega_\nu}{2}e^{-\sigma_\nu x_1/\mu}\int_0^1 p^{(0)}(\mu,-\mu'')\mathcal{J}_\nu{}^{(1)}(x_1;\mu'',\mu')\frac{d\mu''}{\mu''}-\frac{\omega_\nu}{2}e^{-\sigma_\nu x_1/\mu'}\int_0^1\mathcal{J}_\nu{}^{(1)}(x_1;\mu,\mu'')p^{(0)}(\mu'',-\mu')\frac{d\mu''}{\mu''},\end{aligned}$$

$$\begin{aligned}(1/\mu+1/\mu')&\mathcal{S}_\nu{}^{(n)}(x_1;\mu,\mu')\\ =&\frac{\omega_\nu}{2}\int_0^1 p^{(0)}(\mu,\mu'')\mathcal{S}_\nu{}^{(n-1)}(x_1;\mu'',\mu')\frac{d\mu''}{\mu''}-\frac{\omega_\nu}{2}e^{-\sigma_\nu x_1/\mu}\int_0^1 p^{(0)}(\mu,-\mu'')\mathcal{J}_\nu{}^{(n-1)}(x_1;\mu'',\mu')\frac{d\mu''}{\mu''}\\ &+\frac{\omega_\nu}{2}\int_0^1\mathcal{S}_\nu{}^{(n-1)}(x_1;\mu,\mu'')p^{(0)}(-\mu'',-\mu')\frac{d\mu''}{\mu''}-\frac{\omega_\nu}{2}e^{-\sigma_\nu x_1/\mu'}\int_0^1\mathcal{J}_\nu{}^{(n-1)}(x_1;\mu,\mu'')p^{(0)}(\mu'',-\mu')\frac{d\mu''}{\mu''}\\ &+\frac{\omega_\nu}{4}\sum_{r=1}^{n-2}\int_0^1\int_0^1\mathcal{S}_\nu{}^{(r)}(x_1;\mu,\mu'')p^{(0)}(-\mu'',\mu''')\mathcal{S}_\nu{}^{(n-r-1)}(x_1;\mu''',\mu')\frac{d\mu''}{\mu''}\frac{d\mu'''}{\mu'''}\\ &+\frac{\omega_\nu}{4}\sum_{r=1}^{n-2}\int_0^1\int_0^1\mathcal{J}_\nu{}^{(r)}(x_1;\mu,\mu'')p^{(0)}(\mu'',-\mu''')\mathcal{J}_\nu{}^{(n-r-1)}(x_1;\mu''',\mu')\frac{d\mu''}{\mu''}\frac{d\mu'''}{\mu'''},\quad(n\geq 3).\end{aligned} \tag{6}$$

One can deduce analogous relations for $\mathcal{J}_\nu{}^{(n)}$ and $\mathcal{E}_\nu{}^{(n)}$.

In the window region, the solution for a certain wavelength could represent a certain spectral interval around that wavelength, since the related quantities in the window region are all slowly changing with respect to ν. On the other hand, in the band regions, because of the involvement of k_ν in the problem, the final solution should be that averaged over a certain spectral interval. Hence, in order to evaluate $\overline{\mathcal{S}_\nu{}^{(n)}(x_1;\mu,\mu')}$ from (6), it is necessary to evaluate the quantities $\overline{\omega_\nu{}^n}$ and $\overline{\omega_\nu{}^n e^{-\sigma_\nu x_1 g}}$, where g represents functions of $\mu,\mu',\ldots,\mu^{(n)}$ such as $1/\mu$, $1/\mu+1/\mu'$ or $1/\mu+1/\mu'+\cdots+1/\mu^{(n)}$, and the bar means the wavenumber average,

$$\frac{1}{\Delta\nu}\int_{\Delta\nu}\cdots d\nu.$$

Evaluation of $\overline{\omega_\nu{}^n}$ is carried out as follows: By use of the well-known integral

$$\int_0^\infty e^{-\sigma_\nu x}x^{n-1}dx=\frac{(n-1)!}{\sigma_\nu{}^n}, \tag{7}$$

$\omega_\nu{}^n$ is expressed as

$$\begin{aligned}\omega_\nu{}^n&=(\sigma_{s,\nu}/\sigma_\nu)^n\\ &=\frac{\sigma_{s,\nu}{}^n}{(n-1)!}\int_0^\infty e^{-\sigma_\nu x}x^{n-1}dx.\end{aligned} \tag{8}$$

Using (2) and assuming that $\sigma_{s,\nu}$ and $\sigma_{a,\nu}$ are constants with respect to ν in the interval $\Delta\nu$, we have

$$\begin{aligned}\overline{\omega_\nu{}^n}&=\frac{1}{\Delta\nu}\int_{\Delta\nu}\omega_\nu{}^n d\nu\\ &=\frac{\sigma_{s,\nu}{}^n}{(n-1)!}\int_0^\infty e^{-(\sigma_{s,\nu}+\sigma_{a,\nu})x}x^{n-1}\left[\frac{1}{\Delta\nu}\int_{\Delta\nu}e^{-k_\nu x}d\nu\right]dx.\end{aligned} \tag{9}$$

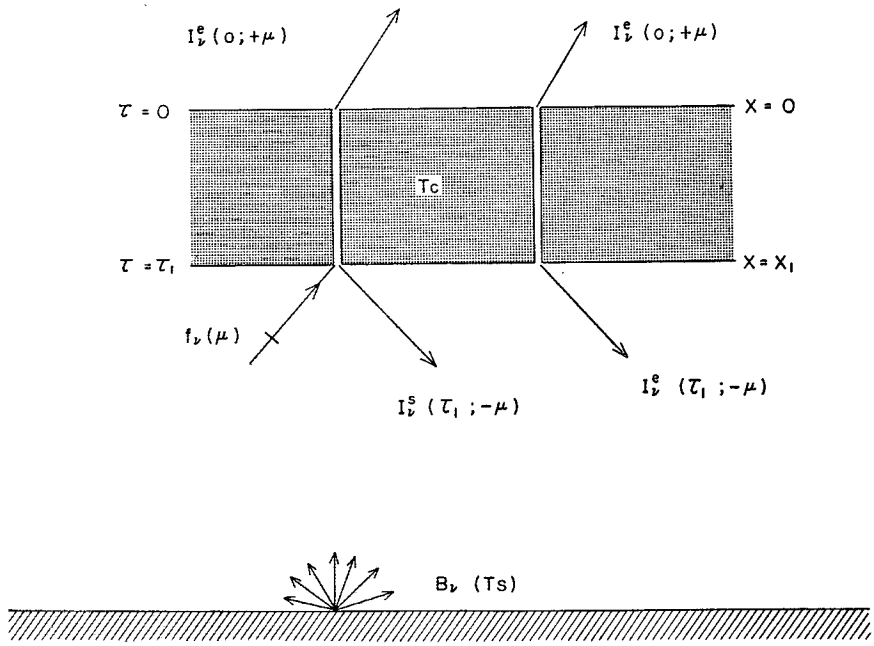

FIG. 3. Cloud model used in this study.

The quantity in the bracket in (9) is just the mean transmission of water vapor in the cloud.

Now, the mean transmission of the infrared band can be expressed with any required accuracy as

$$\frac{1}{\Delta\nu}\int_{\Delta\nu} e^{-k_\nu x}d\nu=\frac{1}{N}\sum_{i=1}^{N} e^{-a_i x}. \tag{10}$$

Putting (10) into (9) and referring to (7), we have

$$\overline{\omega_\nu{}^n}=\frac{1}{N}\sum_{i=1}^{N}\left(\frac{\sigma_{s,\nu}}{\sigma_{s,\nu}+\sigma_{a,\nu}+a_i}\right),$$

$$=\frac{1}{N}\sum_{i=1}^{N}\omega_i{}^n, \tag{11}$$

where

$$\left.\begin{aligned}\omega_i&=(\sigma_{s,\nu}/\sigma_i)\\ \sigma_i&=\sigma_{s,\nu}+\sigma_{a,\nu}+a_i\end{aligned}\right\}. \tag{12}$$

Next, by using (8), $\omega_\nu{}^n e^{-\sigma_\nu x_{1\theta}}$ can be expressed as

$$\omega_\nu{}^n e^{-\sigma_\nu x_{1\theta}}=\frac{\sigma_{s,\nu}{}^n}{(n-1)!}\int_0^\infty t^{n-1}e^{-\sigma_\nu(t+x_{1\theta})}dt. \tag{13}$$

Using (10) and again referring to (8), we get

$$\overline{\omega_\nu{}^n e^{-\sigma_\nu x_{1\theta}}}=\frac{1}{N}\sum_{i=1}^{N}\omega_i{}^n e^{-\sigma_i x_{1\theta}}. \tag{14}$$

In the case of a semi-infinitely thick cloud, the process of obtaining $\overline{\mathbb{S}_\nu{}^{(n)}}$ from (6) is relatively simple, because the terms involving the transmission functions in (6) vanish; accordingly, the integration with respect to ν becomes independent of the integration over directions. The resulting recursion relations which are derived from (6) by use of (11) are given by

$$\left.\begin{aligned}
&(1/\mu+1/\mu')\overline{\mathbb{S}_\nu{}^{(1)}(\mu,\mu')}=\overline{\omega_\nu}\,p^{(0)}(\mu,-\mu')\\
&(1/\mu+1/\mu')\overline{\mathbb{S}_\nu{}^{(2)}(\mu,\mu')}=\frac{1}{2}\frac{\overline{\omega_\nu{}^2}}{\omega_\nu}\int_0^1 p^{(0)}(\mu,\mu'')\overline{\mathbb{S}_\nu{}^{(1)}(\mu'',\mu')}\frac{d\mu''}{\mu''}+\frac{1}{2}\frac{\overline{\omega_\nu{}^2}}{\omega_\nu}\int_0^1\overline{\mathbb{S}_\nu{}^{(1)}(\mu,\mu'')}p^{(0)}(-\mu'',-\mu')\frac{d\mu''}{\mu''}\\
&(1/\mu+1/\mu')\overline{\mathbb{S}_\nu{}^{(n)}(\mu,\mu')}=\frac{1}{2}\frac{\overline{\omega_\nu{}^n}}{\omega_\nu{}^{n-1}}\int_0^1 p^{(0)}(\mu,\mu'')\overline{\mathbb{S}_\nu{}^{(n-1)}(\mu'',\mu')}\frac{d\mu''}{\mu''}+\frac{1}{2}\frac{\overline{\omega_\nu{}^n}}{\omega_\nu{}^{n-1}}\int_0^1\overline{\mathbb{S}_\nu{}^{(n-1)}(\mu,\mu'')}p^{(0)}(-\mu'',-\mu')\frac{d\mu''}{\mu''}\\
&\qquad+\tfrac{1}{4}\sum_{r=1}^{n-2}\frac{\overline{\omega_\nu{}^n}}{\omega_\nu{}^r\omega_\nu{}^{n-r-1}}\int_0^1\int_0^1\overline{\mathbb{S}_\nu{}^{(r)}(\mu,\mu'')}p^{(0)}(-\mu'',\mu''')\,\overline{\mathbb{S}_\nu{}^{(n-r-1)}(\mu''',\mu')}\frac{d\mu''}{\mu''}\frac{d\mu'''}{\mu'''},\quad(n\geq 3)
\end{aligned}\right\}. \tag{15}$$

The recursion relations for $\overline{\mathcal{E}_\nu^{(n)}}$ can also be obtained in a similar way, which are given by

$$\left.\begin{aligned}
&\overline{\mathcal{E}_\nu^{(0)}(\mu)} = (1-\overline{\omega_\nu})B_{\Delta\nu}(Tc)\\
&\overline{\mathcal{E}_\nu^{(1)}(\mu)} = \frac{1}{2}\frac{(\overline{\omega_\nu}-\overline{\omega_\nu^2})}{\overline{\omega_\nu}}B_{\Delta\nu}(Tc)\int_0^1 \overline{\mathcal{S}_\nu^{(1)}(\mu,\mu')}\frac{d\mu'}{\mu'} + \frac{1}{2}\frac{(\overline{\omega_\nu}-\overline{\omega_\nu^2})}{(1-\overline{\omega_\nu})}\int_0^1 p^{(0)}(\mu,\mu')\overline{\mathcal{E}_\nu^{(0)}(\mu')}d\mu'\\
&\overline{\mathcal{E}_\nu^{(n)}(\mu)} = \frac{1}{2}\frac{(\overline{\omega_\nu^n}-\overline{\omega_\nu^{n+1}})}{\overline{\omega_\nu^n}}B_{\Delta\nu}(Tc)\int_0^1 \overline{\mathcal{S}_\nu^{(n)}(\mu,\mu')}\frac{d\mu'}{\mu'} + \frac{1}{2}\frac{(\overline{\omega_\nu^n}-\overline{\omega_\nu^{n+1}})}{(\overline{\omega_\nu^{n-1}}-\overline{\omega_\nu^n})}\int_0^1 p^{(0)}(\mu,\mu')\overline{\mathcal{E}_\nu^{(n-1)}(\mu')}d\mu'\\
&\qquad + \tfrac{1}{4}\sum_{r=1}^{n-1}\frac{(\overline{\omega_\nu^n}-\overline{\omega_\nu^{n+1}})}{\overline{\omega_\nu^r}(\overline{\omega_\nu^{n-r-1}}-\overline{\omega_\nu^{n-r}})}\int_0^1\int_0^1 \overline{\mathcal{S}_\nu^{(r)}(\mu,\mu')}p^{(0)}(\mu',-\mu'')\overline{\mathcal{E}_\nu^{(n-r-1)}(\mu'')}\frac{d\mu'}{\mu'}d\mu'', \quad (n\geq 2)
\end{aligned}\right\} \tag{16}$$

The equations for $\overline{\mathcal{T}_\nu^{(n)}}$ do not appear in this case.

In the case of a cloud of finite optical thickness, $\overline{\mathcal{S}_\nu^{(n)}}$, for instance, can be derived from (6) by using (14). However, as $\overline{\omega_\nu^n e^{-\sigma_\nu x_1/\mu}}$ depends on $\mu,\mu', \cdots, \mu^{(n)}$, the exact formula for $\overline{\mathcal{S}_\nu^{(n)}}$ becomes complicated for large n, containing many terms which involve multiple integrals over directions. Therefore, an approximate method of estimating $\overline{\mathcal{S}_\nu^{(n)}}$ becomes necessary for large n.

Taking the average of (6) with respect to ν and using the mean value theorm of integral, we have

$$\begin{aligned}
(1/\mu+1/\mu')\overline{\mathcal{S}_\nu^{(n)}(x_1;\mu,\mu')} &= \tfrac{1}{2}\alpha_n\int_0^1 p^{(0)}(\mu,\mu'')\overline{\mathcal{S}_\nu^{(n-1)}(x_1;\mu'',\mu')}\frac{d\mu''}{\mu''} + \tfrac{1}{2}\alpha_n'\int_0^1 \overline{\mathcal{S}_\nu^{(n-1)}(x_1;\mu,\mu'')}p^{(0)}(-\mu'',-\mu')\frac{d\mu''}{\mu''}\\
&\quad -\tfrac{1}{2}\beta_n(\mu)\int_0^1 p^{(0)}(\mu,-\mu'')\overline{\mathcal{J}_\nu^{(n-1)}(x_1;\mu'',\mu')}\frac{d\mu''}{\mu''} - \tfrac{1}{2}\beta_n'(\mu')\int_0^1 \overline{\mathcal{J}_\nu^{(n-1)}(x_1;\mu,\mu'')}p^{(0)}(\mu'',-\mu')\frac{d\mu''}{\mu''}\\
&\quad +\tfrac{1}{4}\sum_{r=1}^{n-2}\gamma_{n,r}\int_0^1\int_0^1 \overline{\mathcal{S}_\nu^{(r)}(x_1;\mu,\mu'')}p^{(0)}(-\mu'',\mu''')\overline{\mathcal{S}_\nu^{(n-r-1)}(x_1;\mu''',\mu')}\frac{d\mu''}{\mu''}\frac{d\mu'''}{\mu'''}\\
&\quad -\tfrac{1}{4}\sum_{r=1}^{n-2}\gamma_{n,r}'\int_0^1\int_0^1 \overline{\mathcal{J}_\nu^{(r)}(x_1;\mu,\mu'')}p^{(0)}(\mu'',-\mu''')\overline{\mathcal{J}_\nu^{(n-r-1)}(x_1;\mu''',\mu')}\frac{d\mu''}{\mu''}\frac{d\mu'''}{\mu'''},
\end{aligned} \tag{17}$$

where

$$\alpha_n = \int_0^1 p^{(0)}(\mu,\mu'')\overline{\omega_\nu\mathcal{S}_\nu^{(n-1)}(x_1;\mu'',\mu')}\frac{d\mu''}{\mu''} \Big/ \int_0^1 p^{(0)}(\mu,\mu'')\overline{\mathcal{S}_\nu^{(n-1)}(x_1;\mu'',\mu')}\frac{d\mu''}{\mu''}, \tag{18}$$

$$\beta_n(\mu) = \int_0^1 p^{(0)}(\mu,-\mu'')\overline{\omega_\nu e^{-\sigma_\nu x_1/\mu}\mathcal{J}_\nu^{(n-1)}(x_1;\mu'',\mu')}\frac{d\mu''}{\mu''} \Big/ \int_0^1 p^{(0)}(\mu,-\mu'')\overline{\mathcal{J}_\nu^{(n-1)}(x_1;\mu'',\mu')}\frac{d\mu''}{\mu''}, \tag{19}$$

$$\begin{aligned}
\gamma_{n,r} = \int_0^1\int_0^1 \overline{\omega_\nu\mathcal{S}_\nu^{(r)}(x_1;\mu,\mu'')\mathcal{S}_\nu^{(n-r-1)}(x_1;\mu''',\mu')}p^{(0)}(-\mu'',\mu''')\frac{d\mu''}{\mu''}\frac{d\mu'''}{\mu'''} \Big/\\
\int_0^1\int_0^1 \overline{\mathcal{S}_\nu^{(r)}(x_1;\mu,\mu'')}p^{(0)}(-\mu'',\mu''')\overline{\mathcal{S}_\nu^{(n-r-1)}(x_1;\mu''',\mu')}\frac{d\mu''}{\mu''}\frac{d\mu'''}{\mu'''},
\end{aligned} \tag{20}$$

and we have similar formulae for α_n', β_n' and $\gamma_{n,r}'$. The exact evaluation of these quantities is very difficult. Therefore, our problem is how to approximate them in simple forms. From Eqs. (6) and (15) it can easily be seen that the function $S_\nu^{(n)}(x_1;\mu,\mu')$ given by (3) tends to become independent of ν when x_1 becomes large. For small values of x_1, this does not hold. However, if we assume that $S_\nu^{(n)}$ is independent of ν for every value of x_1, we have

$$\alpha_n = \alpha_n' = \overline{\omega_\nu^n}/\overline{\omega_\nu^{n-1}}, \tag{21}$$

$$\beta_n(\mu) = \beta_n'(\mu) = \overline{\omega_\nu^n e^{-\sigma_\nu x_1/\mu}}/\overline{\omega_\nu^{n-1}}, \tag{22}$$

$$\gamma_{n,r} = \gamma_{n,r}' = \overline{\omega_\nu^n}/(\overline{\omega_\nu^r}\,\overline{\omega_\nu^{n-r-1}}). \tag{23}$$

We will use this approximation for $n>3$, and the following exact expressions for $\overline{\mathcal{S}_\nu^{(n)}}$ together with (14) will be used for $n\leq 3$:

$$\left.\begin{aligned}
(1/\mu+1/\mu')\overline{\mathcal{S}_\nu^{(1)}(x_1;\mu,\mu')} &= \overline{\omega_\nu\{1-\exp[-\sigma_\nu x_1(1/\mu+1/\mu')]\}}p^{(0)}(\mu,-\mu') \\
(1/\mu+1/\mu')\overline{\mathcal{S}_\nu^{(2)}(x_1;\mu,\mu')} &= \frac{1}{2}\int_0^1 p^{(0)}(\mu,\mu'')p^{(0)}(\mu'',-\mu')\overline{\omega_\nu^2\{1-\exp[-\sigma_\nu x_1(1/\mu'+1/\mu'')]\}}\frac{\mu'}{\mu'+\mu''}d\mu'' \\
&+\frac{1}{2}\int_0^1 p^{(0)}(\mu,-\mu'')p^{(0)}(-\mu'',-\mu')\overline{\omega_\nu^2\{1-\exp[-\sigma_\nu x_1(1/\mu+1/\mu'')]\}}\frac{\mu}{\mu+\mu''}d\mu'' \\
&-\frac{1}{2}\int_0^1 p^{(0)}(\mu,-\mu'')p^{(0)}(-\mu'',-\mu')\overline{\omega_\nu^2 e^{-\sigma_\nu x_1/\mu}[e^{-\sigma_\nu x_1/\mu'}-e^{-\sigma_\nu x_1/\mu''}]}\frac{\mu'}{\mu'-\mu''}d\mu'' \\
&-\frac{1}{2}\int_0^1 p^{(0)}(-\mu,-\mu'')p^{(0)}(\mu'',-\mu')\overline{\omega_\nu^2 e^{-\sigma_\nu x_1/\mu'}[e^{-\sigma_\nu x_1/\mu''}-e^{-\sigma_\nu x_1/\mu}]}\frac{\mu}{\mu''-\mu}d\mu''
\end{aligned}\right\}, \quad (24)$$

etc.

This approximation is justified because of the fact that the contribution of higher order scattering to the law of diffuse reflection is negligible in the case of a thin cloud, and that in the case of a thick cloud, in which higher order scattering is important, the accuracy of this present approximation increases. Similar approximations can also be made for $\overline{\mathcal{J}_\nu^{(n)}}$ and $\overline{\mathcal{E}_\nu^{(n)}}$.

If $\overline{\mathcal{S}_\nu^{(n)}}$, $\overline{\mathcal{J}_\nu^{(n)}}$ and $\overline{\mathcal{E}_\nu^{(n)}}$ are evaluated, then from (3), (4), (5) and definitions of the scattering, transmission and emission function [Eqs. (10), (11) and (18) of the paper by Yamamoto *et al.*], we can evaluate the wavenumber-averaged emergent intensities, and can finally evaluate the mean reflectivity, transmissivity and emissivity over the interval $\Delta\nu$; these are defined, respectively, by

$$r_{\Delta\nu}=2\pi\int_0^1 \overline{I_\nu^s(x_1;-\mu)}\mu d\mu/\pi B_{\Delta\nu}(T_s), \quad (25)$$

$$t_{\Delta\nu}=2\pi\int_0^1 \overline{I_\nu^s(0;+\mu)}\mu d\mu/\pi B_{\Delta\nu}(T_s), \quad (26)$$

$$e_{\Delta\nu}=2\pi\int_0^1 \overline{I_\nu^e(0;+\mu)}\mu d\mu/\pi B_{\Delta\nu}(T_e). \quad (27)$$

Before closing this section, we shall briefly describe the mean transmission function of water vapor given by (10). In this investigation, Cowling's (1950) absorption curve, which is expressed as a function of $l_\nu u/2$ in Fig. 4, is used, where l_ν is the generalized absorption coefficient of Elsasser and u the effective path length of water vapor given by

$$u=\frac{1}{g}\int_0^p \frac{p}{p_0}dp, \quad (28)$$

where the symbols have the usual meanings. For the values of l_ν, those estimated by Wark *et al.* (1962) are used. Application of this approximate method for the estimation of the water vapor transmission is reasonable, because water clouds are considered to appear in the middle and lower parts of the troposphere.

Cowling's absorption curve is then fitted by using ten exponential terms as given by (10). The results are shown by the broken curve in Fig. 4.

4. Results

The drop-size distribution of our cloud model is that of altostratus measured by Diem. (1948). It has a minimum, maximum and mode diameter at 2, 26 and 9 μ, respectively. The number density of this cloud model is 450 cm^{-3} and the water content 0.28 gm m^{-3}.

Numerical computations have been carried out on cloud models with various thicknesses. Cloud temperature was assumed to be -10C and the surface temperature of the earth was assumed to be 15C. The effective water vapor content in the cloud is 1.44 gm m^{-3}, which is estimated from the saturation vapor amount at the

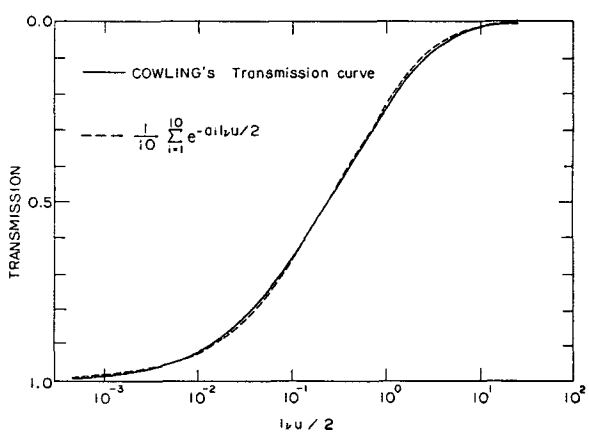

FIG. 4. Water vapor transmission as a function $l_\nu u/2$. Solid line shows Cowling's transmission curve, and the broken line, the approximation (10) with $N=10$. Values of a_i are as follows: a_i =0.20141, 0.63093, 1.24536, 1.45326, 2.18506, 3.23208, 3.38774, 7.43775, 11.30550 and 82.09177.

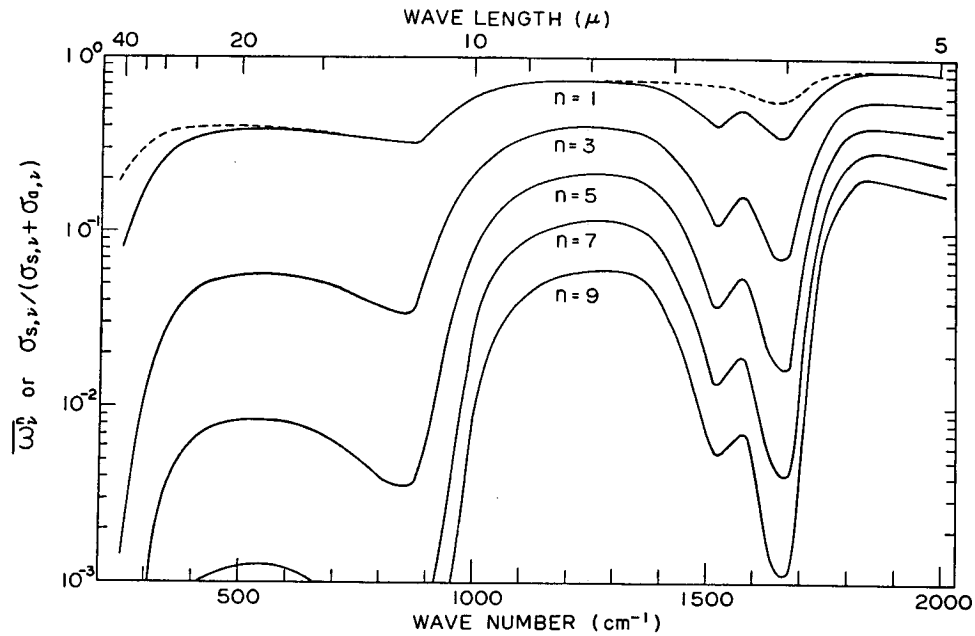

FIG. 5. $\overline{\omega_\nu{}^n}$ for various values of η vs wavelength. Broken line shows the albedo for single scattering due to cloud droplets alone, $\sigma_{s,v}/(\sigma_{s,v}+\sigma_{a,v})$.

cloud temperature and pressure. The spectral interval for averaging is taken to be 50 cm^{-1}.

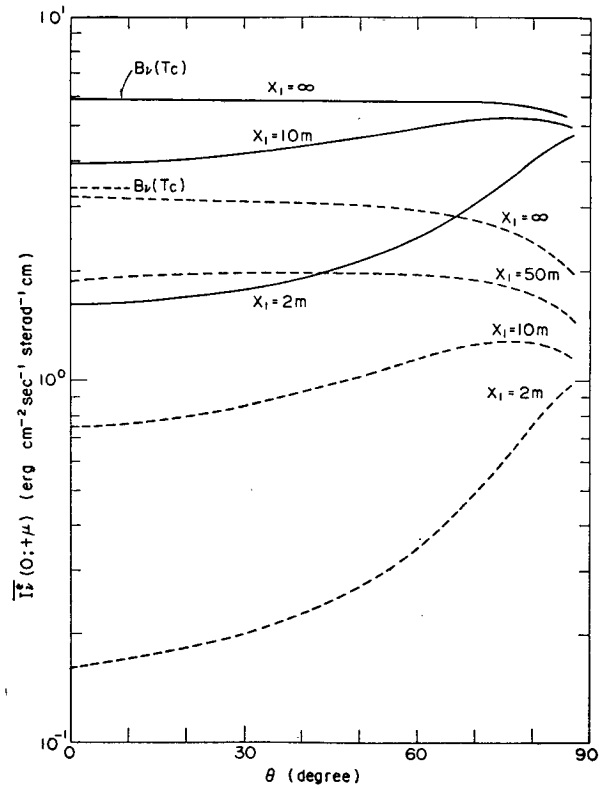

FIG. 6. Angular distribution of the emitted radiation for the spectral intervals 1650–1700 cm^{-1} (solid lines) and 1800–1850 cm^{-1} (broken lines), as a function of θ.

To evaluate the integrals which appear in (15) and other equations, we adopt a direct numerical computation based on Gauss's quadrature formula, where the integrals are divided into 9 parts for the incident direction and 10 for the scattered direction.

The maximum order of scattering, up to which computation was carried out, is 4-th order for the thinnest cloud (x_1=2m) and 30-th for the semi-infinitely thick cloud.

Fig. 5 shows the effect of absorption by water vapor in the cloud on the albedo for single scattering. In the 6.3 μ band and the rotational band, $\overline{\omega_\nu}$ ($=\overline{\omega_\nu{}^1}$), the albedo due to both cloud droplets and water vapor is smaller than that due to cloud droplets alone (broken line).

Fig. 5 also shows the values of $\overline{\omega_\nu{}^n}$ for various values of n. It will be seen in the figure that at a given wavenumber $\overline{\omega_\nu{}^n}$ decreases nearly exponentially with increase of n.

Fig. 6 shows the angular distribution of the emitted radiation, $\overline{I_\nu{}^e(0;+\mu)}$ or $\overline{I_\nu{}^e(x_1;-\mu)}$, from clouds of various thicknesses at two spectral intervals; namely, 1650–1700 cm^{-1} (strong absorption region) and 1800–1850 cm^{-1} (weak absorption region) as a function of the polar angle θ. It is also seen in Fig. 6 that the emitted radiation from the cloud is larger at the strong absorption region than at the weak absorption region, and that when the cloud is thin, the emitted radiation assumes limb brightening, but when the cloud becomes thick it turns to limb darkening. Moreover, it is noticed that the emitted radiation from the semi-infinitely thick cloud approaches $B_\nu(Tc)$ at 1650–1700 cm^{-1} where ab-

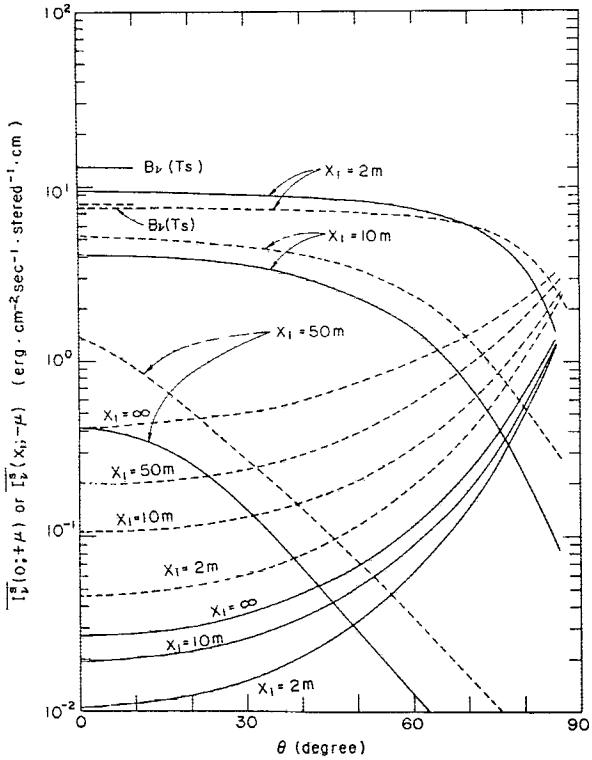

FIG. 7. Angular distribution of the reflected and transmitted radiation for the spectral intervals 1650-1700 cm^{-1} (solid lines) and 1800–1850 cm^{-1} (broken lines), as a function of θ. Curves exhibiting limb-brightening show the reflected radiation, and limb-darkening, the transmitted radiation.

sorption is strong, while it is less than $B_\nu(Tc)$ at 1800–1850 cm^{-1} where absorption is weak. It will be necessary to make some comment on these features.

In an atmosphere in local thermodynamic equilibrium without scattering ($\omega_\nu=0$), the solution of the equation of radiative transfer under the boundary conditions shown in Fig. 3 becomes

$$I_\nu^e(0;+\mu)=B_\nu(Tc)[1-e^{-\sigma_\nu x_1/\mu}]. \qquad (29)$$

This solution indicates limb brightening, the degree of which becomes smaller with increase of thickness. It also indicates the emitted radiation tending toward $B_\nu(Tc)$ for an infinitely thick cloud. The reason why the emitted radiation shows limb brightening when the cloud is thin is explained by (29), because scattering is negligible in the thin cloud. With increase of cloud thickness, the role of ω_ν or of multiple scattering becomes important in the process of radiative transfer so that emission from the cloud is depressed by multiple scattering to some extent. This is revealed as limb darkening for thick cloud and also as the shortage of emission from $B_\nu(Tc)$ in the semi-infinitely thick cloud.

Fig. 7 shows the angular distribution of the reflected radiation, $\overline{I_\nu^s(x_1;-\mu)}$, and that of the transmitted radiation, $\overline{I_\nu^s(0;+\mu)}$. From the figure it can be seen that the reflected radiation increases with increase of cloud thickness, that it is stronger in the interval 1800–1850 cm^{-1} than 1650–1700 cm^{-1} for the same cloud, and that its angular distribution shows limb brightening.

It can also be seen that the transmitted radiation, $\overline{I_\nu^s(0;+\mu)}$, decreases rapidly with increase of cloud thickness, that it is stronger in the interval 1800–1850 cm^{-1} than 1650–1700 cm^{-1} for the same cloud, and that its angular distribution shows limb darkening.

Fig. 8 shows the angular distribution of the total emergent radiation, i.e., $\overline{I_\nu(0;+\mu)}$ and $\overline{I_\nu(x_1;-\mu)}$, where

$$\overline{I_\nu(0;+\mu)}=\underbrace{\overline{I_\nu^e(0;+\mu)}}_{\text{emitted radiation}}+\underbrace{\overline{I_\nu^s(0;+\mu)}}_{\text{transmitted radiation}},$$

$$\overline{I_\nu(x_1;-\mu)}=\underbrace{\overline{I_\nu^e(x_1;-\mu)}}_{\text{emitted radiation}}+\underbrace{\overline{I_\nu^s(x_1;-\mu)}}_{\text{reflected radiation}}.$$

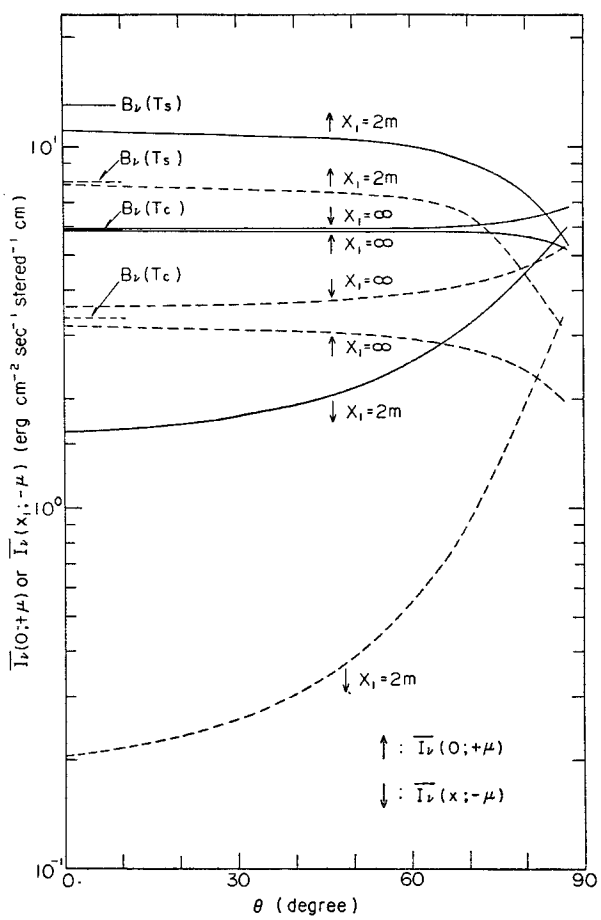

FIG. 8. Angular distribution of total emergent radiation from the top or base of clouds of various thicknesses. The upward arrow shows the emergent radiation from the cloud top, and the downward arrow, that from the cloud base. Solid and broken lines correspond to the spectral intervals 1650–1700 cm^{-1} and 1800–1850 cm^{-1}, respectively.

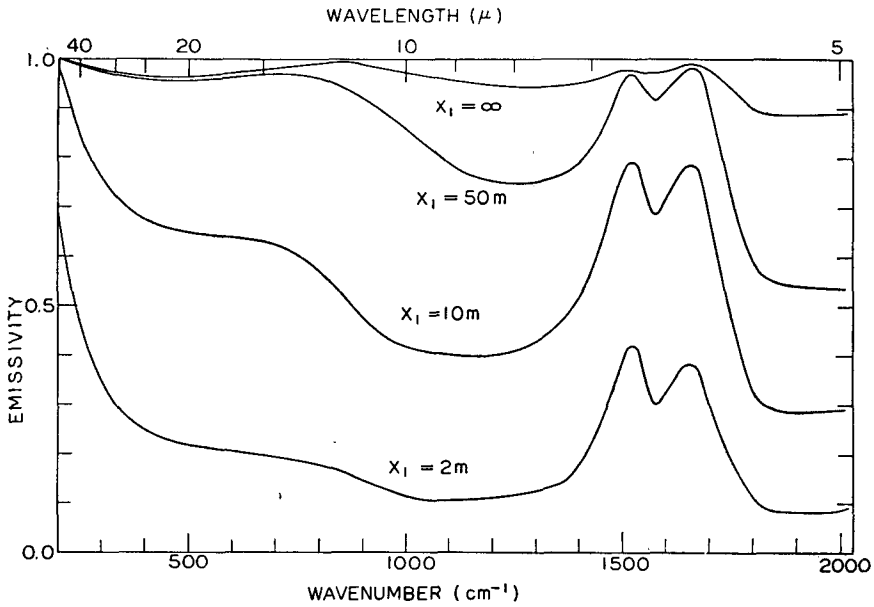

FIG. 9. Spectral emissivity of clouds of various thicknesses vs wavenumber or wavelength.

When the cloud is thin ($x_1=2$ m), $\overline{I_\nu(0;+\mu)}$ or the emergent radiation from the cloud top is mainly due to $\overline{I_\nu^s(0;+\mu)}$, and accordingly assumes limb darkening as in the case of Fig. 7. When the cloud becomes thick (as in the case of $x_1=\infty$, also shown in the figure), the emergent radiation is mostly composed of the emitted radiation and shows weak limb darkening as in the case of Fig. 6.

On the other hand, the downward radiation from the cloud base shows limb brightening both for thin ($x_1=2$ m) and thick ($x_1=\infty$) clouds. When the cloud is thin, both the emitted and reflected radiations

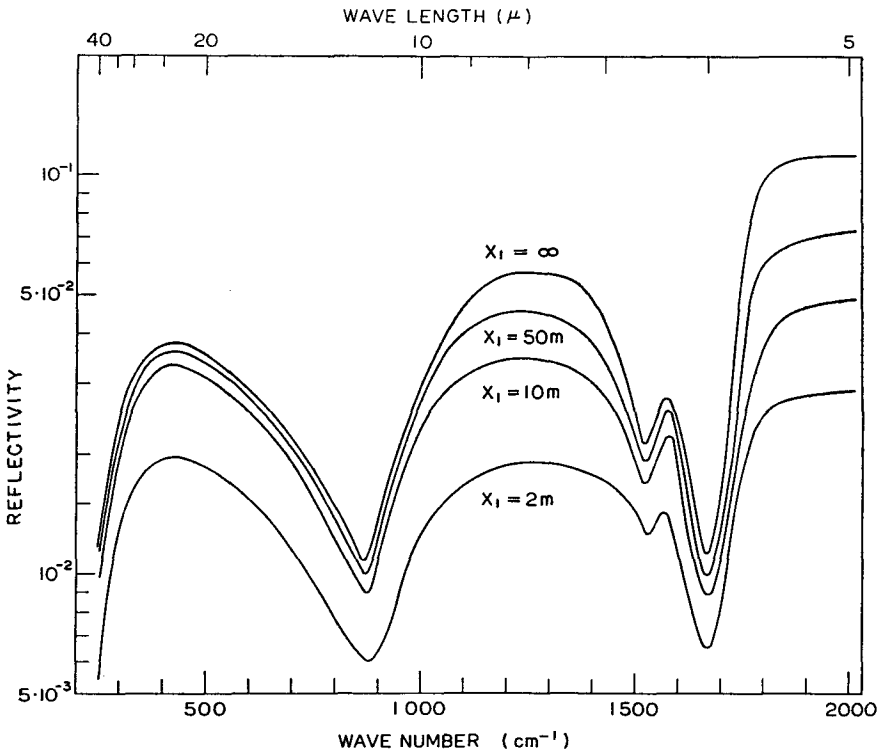

FIG. 10. Spectral reflectivity of clouds of various thicknesses vs wavenumber or wavelength.

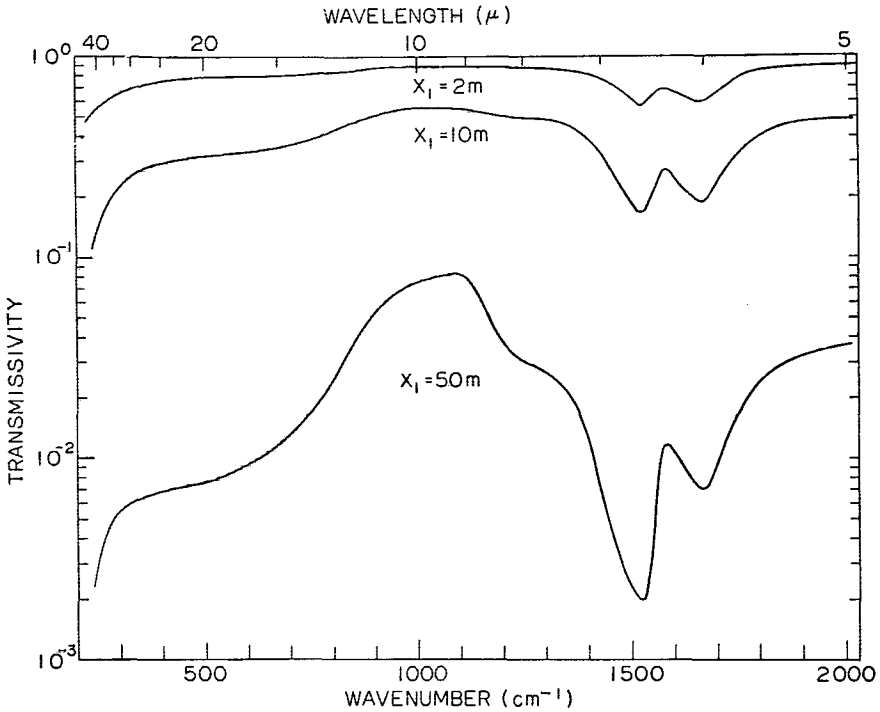

FIG. 11. Spectral transmissivity of clouds of various thicknesses vs wavenumber or wavelength.

assume limb brightening as shown in Figs. 6 and 7, so that it is natural that the resultant downward radiation shows limb brightening. In the case of the thick cloud ($x_1 - \infty$), limb brightening of downward radiation is due to the contribution of the reflected radiation at the cloud base.

Fig. 9 shows the emissivity of clouds of various thicknesses as a function of wavenumber. It is noticed in the figure that emissivity increases with increase of cloud thickness, but is smaller than unity even for an infinitely thick cloud at any spectral region. It is also noticed that emissivity is small in the window regions around 5 μ and 7 10 μ, and is large in the 6.3 μ band region, in the region around 12 μ, and in the far infrared region. The large emissivity value around 12 μ corresponds to a minimum of the albedo for single scattering which exists in this region as shown in Fig. 5.

Reflectivity, defined by (25), of clouds of various thicknesses is shown in Fig. 10 as a function of wavenumber. As seen in the figure, reflectivity increases with increase of cloud thickness and shows small values in the 6.3 μ, 12 μ and far infrared regions, where emissivity assumes large values.

From Figs. 9 and 10 it can be seen, in the case of a semi-infinitely thick cloud, that the sum of emissivity and reflectivity is equal to unity at any spectral region. This is the Kirchhoff's law and it suggests the accuracy of our calculation.

Transmissivity of clouds of various thicknesses defined by (6) is shown in Fig. 11 which indicates that transmissivity decreases with increase of cloud thickness and that it is smaller in the 6.3 μ band region and in the far infrared region.

The mean emissivity, reflectivity and transmissivity of the cloud for the entire infrared region are given in the forms

$$\tilde{\mathcal{E}} = \sum_i e_{\Delta\nu,i} B_{\Delta\nu,i}(Tc) / \sum_i B_{\Delta\nu,i}(Tc), \tag{30}$$

$$\tilde{\mathcal{R}} = \sum_i r_{\Delta\nu,i} B_{\Delta\nu,i}(Ts) / \sum_i B_{\Delta\nu,i}(Ts), \tag{31}$$

$$\tilde{\mathcal{J}} = \sum_i t_{\Delta\nu,i} B_{\Delta\nu,i}(Ts) / \sum_i B_{\Delta\nu,i}(Ts), \tag{32}$$

where $e_{\Delta\nu,i}$, $r_{\Delta\nu,i}$ and $t_{\Delta\nu,i}$ are given by (25)–(27) and

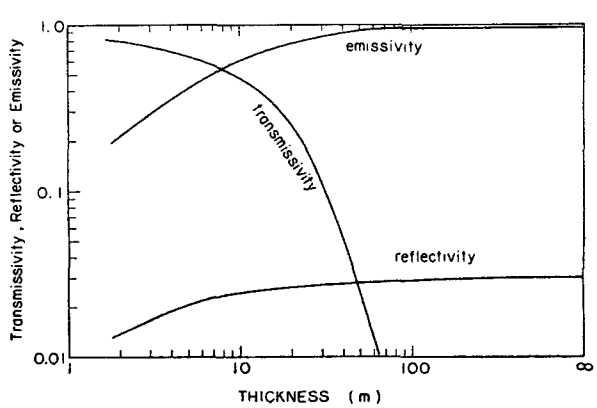

FIG. 12. Emissivity, reflectivity and transmissivity of clouds for the infrared region from 5–50 μ vs cloud thickness in meters.

$B_{\Delta\nu,i}$ is the Planck radiance for each spectral interval $\Delta\nu i$.

In Fig. 12, $\tilde{\mathcal{E}}$, $\tilde{\mathcal{R}}$ and $\tilde{\mathcal{J}}$ for the 5–50 μ region are shown as a function of cloud thickness. The mean emissivity and reflectivity tend to 0.97 and 0.030, respectively, as cloud thickness tends to infinity. The mean transmissivity tends, of course, to zero as the thickness tends to infinity.

REFERENCES

Centeno, M., 1941: The refractive index of liquid water in the near infrared spectrum. *J. Opt. Soc. Amer.*, **31**, 244–247.

Chandrasekhar, S., 1950: *Radiative Transfer*. Oxford University Press, 393 pp.

Cowling, T. G., 1950: Atmospheric absorption of heat radiation by water vapor. *Phil. Mag.*, **41**, 109–123.

Diem, M., 1948: Messungen der Grosse von Wolkenelementen II. *Meteor. Rundschau*, **9** and **10**, 261–273.

Dorsey, N. E., 1940: *Properties of Ordinary Water Substance*. New York, Reinhold, 673 pp.

Draegert, D. A., N. W. B. Stone, B. Curnutte and D. Williams, 1966: Far-infrared spectrum of liquid water. *J. Opt. Soc. Amer.*, **56**, 64–69.

Irvine, W. M., and J. B. Pollack, 1968: Infrared optical properties of water and ice spheres. *Icarus*, **8**, 342–360.

Kislovskii, L. D., 1959: Optical characteristics of water and ice in the infrared and radiowave region of the spectrum. *Opt. Spect.* (English Transl.), **7**, 201–206.

Plyler, E. K., and N. Acquista, 1954: Infrared absorption of liquid water from 2 to 42 microns. *J. Opt. Soc. Amer.*, **44**, 505–508.

Pontier, L., and C. Dechambenoy, 1966: Détermination des constantes optiques de l'eau liquide entre 1 et 40 μ. Application au calcul de son pouvior réflecteur et de son émissivité. *Ann. Géophys.*, **22**, 633–641.

Wark, D. Q., G. Yamamoto and J. Lienesch, 1962: Methods of estimating infrared flux and surface temperature from meteorological satellites. *J. Atmos. Sci.*, **19**, 369–384.

Yamamoto, G., M. Tanaka and K. Kamitani, 1966: Radiative transfer in water clouds in the 10-micron window region. *J. Atmos. Sci.*, **23**, 305–313.